Staggered Magnetic Nanowire Devices for Effective Domain Wall Pinning in Racetrack Memory

M. Al Bahri[1], B. Borie[2], T.L. Jin,[3] R. Sbiaa[1], M. Kläui, [2] and S. N. Piramanayagam[3]

[1]*Department of Physics, Sultan Qaboos University, P.O. Box 36, PC 123, Muscat, Oman.*

[2]*Institut für Physik, Johannes Gutenberg-Universität Mainz, Staudinger Weg 7, 55128 Mainz, Germany.*

[3]*Division of Physics and Applied Physics, School of Physical and Mathematical Sciences, Nanyang Technological University, Singapore.*

Domain wall memory devices, wherein the information is stored in nanowires, are believed to replace hard disk drives. A problem that remains to be solved in domain wall memory is to pin the domain walls in a controllable manner at the nanometer scale using simple fabrication. Here, we demonstrate the possibility to stabilize domain walls by making staggered nanowires. Controllable domain wall movement is exhibited in permalloy nanowires using magnetic fields, where the pinning field is about 10 mT. The pinning field and stability of the domain walls can be increased by adjusting the offset dimensions of the staggered nanowires. Domain wall velocities (DWV) of about 200 m/s are computed for the experimentally used permalloy nanowires. DWV were found to be independent of pinning strength and stability, providing a way to tune the pinning without compromising DWV.

PACS number: 75.76.+j, 68.35.Rh, 75.78.F

I. INTRODUCTION

Recently, magnetic domain wall (DW) propagation in nanowires has been the subject of intensive investigations [1–18] because of its fundamental interest in nanomagnetism and potential applications. For instance, DW-based devices have been proposed for high capacity storage [8,9,14], microwave generators [19–25], logic devices [1,2,6,7,26,27] and sensing applications [10,28,29]. The motion of a DW can be driven by a magnetic field or a spin polarized current [30]. In many of these applications, however, controlling the DW dynamics and its position within the nanowire is crucial. For high-density domain wall based memory, several issues regarding the device performance such as thermal stability, power consumption and operation speed need to be solved. Thermally stable recorded data require keeping DW at a precise position within the nanowire for a certain period, which could be a few years if the data are archived. Artificial nanowires (NW) with naturally formed defect of different geometries acting as trapping sites have also been investigated using both numerical simulation and experimental observations [3,31–33]. Several studies have also reported that creating notches experimentally using lithography help to block or pin domain wall [5,34–43]. These artificial constrictions work as pinning sites for DW due to their higher pinning potential than that of other pinning sites such as defects in the NWs. In their work, Bogart *et al.* reported that DW pinning is sensitive to the wall type and its chirality spin structure [37]. Benganza *et al.* investigated DW pinning in FeCoCu nanowires grown by electroplating in alumina templates [38]. They demonstrated the possibility to control DW by applying an external magnetic field. There are also other proposals to use non-geometrical approaches, such as notches, to pin domain walls [44,45]. In this paper, we propose and demonstrate experimentally a new scheme in which the domain wall pinning strength is controlled precisely using a new concept of staggered nanowires. The proposed scheme has several advantages; First of all, the proposed scheme is easy to fabricate as it involves two simple wires which are partially overlapping at the edges. Secondly, as we will show later, the pinning strength can be easily adjusted by changing the depth of step (d) and length of step (l). Furthermore, this device could be made into a multiple bit per cell memory or a domain wall memory, based on the number of segments, as shown in Fig. 1.

II. SAMPLE FABRICATION AND CHARACTERIZATION

The samples of the type $Ni_{81}Fe_{19}$ (30 nm)/Ta (5 nm) were deposited on thermally oxidized Si substrate using DC-magnetron sputtering in a chamber with an argon pressure of 5.7×10^{-3} mbar at a deposition rate of 0.1 nm/s. The hysteresis loop for permalloy thin films was measured by superconducting quantum interference device (SQUID). Staggered nanowires with width of 200 nm were patterned by electron beam lithography

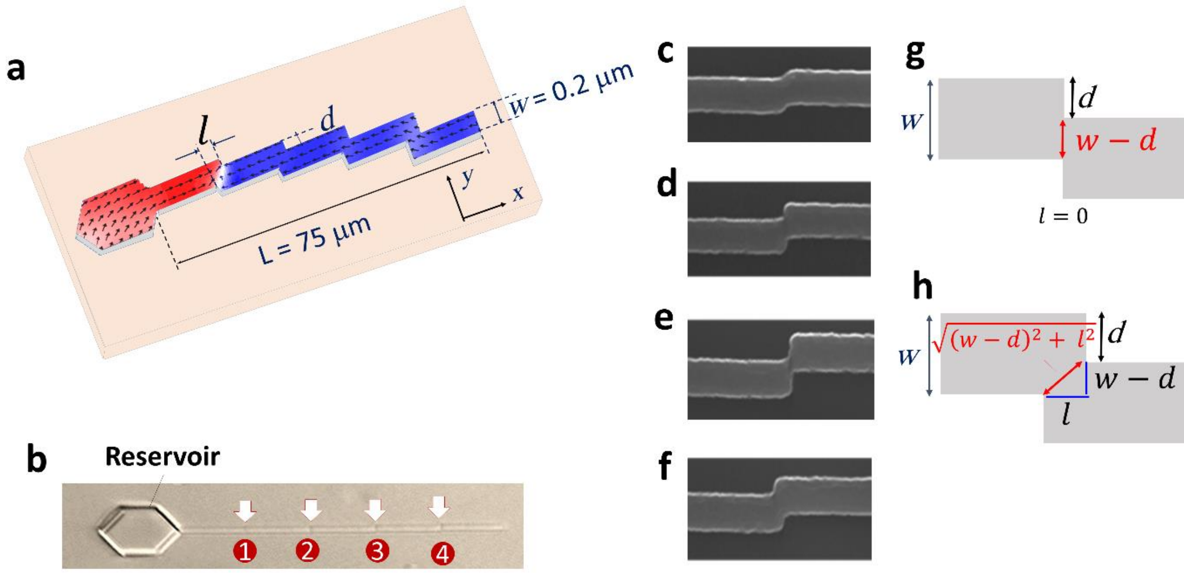

FIG. 1. (Color online) (a) Schematic representation of the device with multi-staggered nanowire. The off-set in x and y direction are defined by l and d, respectivelly. The large pad is for nucleation of domain wall with a smaller magnetic field than the one used for moving it from one pinning region to the other. (b) Optical image of the lithographically fabricated device. The numbers indicate the pinning regions. (c-f) Scanning electron micrograph images of the devices after electron beam lithography and ion beam etching. The images show wires with different off-set values d and l. (g-h) illustration of a junction of the stagerred region with emphasis on the distance between the two corners of the junction. The diagonal, $\sqrt{(w-d)^2+l^2}$, shown in (h) is related to the pinning strength and the type of domain as will be explained in the simulation part.

using a negative resist and ion beam etching. The nanowire was connected with nucleation pad at one of its end. Figure 1 shows a schematic of proposed DW device. As shown in Fig. 1(a), the nanowire has several segments, offset from each other by a distance d from the previous segment in the y direction. The new segment may also be overlapping with the previous segment in the x direction by a distance "l". The DW nanowire in our experiment also has a reservoir at the left end, to create domains at lower fields, and to avoid the formation of reversed domains in the segments of nanowires. Two types of nanowire were fabricated, viz., nanowires with identical steps size and nanowires with different values of d and l as shown in Fig 6. According to values of d and l, eight nanowires were fabricated having same stepped area, four nanowires were with l = 0 nm and d = 50 nm, 100 nm, 150 nm and 200 nm. Other four with l = 50 nm and d = 50 nm, 100 nm, 150 nm and 200 nm.

For the proof-of-concept, we have carried out investigations in such geometries based on NiFe. For high-density applications, materials with a perpendicular magnetic anisotropy may be investigated.

III. RESULTS

We show in Fig. 1 (b), an optical microscope image of the fabricated device. We can clearly see the reservoir in the optical microscope image. We also show the offset regions in the optical microscope by numbers for convenience. In figures 1(c-f), we show Scanning Electron Microscope (SEM) images of offset regions of several devices with different *d* and l values. We can notice that the overlap of the junction region is varying as *d* and *l* are varied, and we will show that the parameters of this region, in particular, the diagonal $\sqrt{(w-d)^2+l^2}$ shown in figure 1(h), determines the pinning strength.

In figure 2(a), we show the optical images of one of the preliminary devices based on NiFe (30 nm), which had the same value of *l* (50 nm) and *d* (50 nm) at all the junctions. To study the pinning effect of such a device, we saturated the sample at first, in a particular direction with an applied magnetic field of 30 mT. Then, we applied a reversal field in steps of 1 mT continuously, until we observe a reversed domain. In Figure 2(b), we show the formation of such a reversed domain with the application of a reversal field (9 mT). Then, we increased the reversal field further in order to depin the domain wall from the first junction. However, when the reversal field was about 18 mT, we noticed that the domain wall did not stop at the second junction but moved rapidly to the end of the nanowire (Fig. 2(c)). Since the pinning field strength depends strongly on the values of *d* and *l*, and since the values of *d* and *l* are uniform at all the junctions, they have the same pinning field strength. Therefore, for an applied

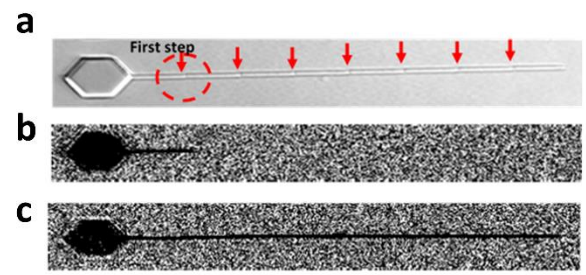

FIG. 2. (a) An optical image of the fabricated device showing the reservoir magnetic area where the domain wall is first created. The arrows show the different staggered regions where domain wall could be stabilized/pinned. In this case *d* and *l* were the same in each step. (b-c) two magneto-optical images for the device where the domain wall is pinned at the first step (b) then moved to the end of the device (c).

magnetic field stronger than the pinning field strength, the domain walls are not pinned at the other junctions. These results indicate that this design of staggered nanowires does not allow for controlled pinning at the different junctions, particularly when we study the field-driven domain wall motion.

As the next step, we fabricated 20 nm-thick NiFe based staggered nanowires with increasing values of *d* from left to right, by keeping the value of *l* fixed in a nanowire. We also fabricated several nanowires with various values of *l*. Figure 3 (a) shows the microscopic image and MOKE images for nanowire with step dimensions of *l* = 0 nm and various *d* values (the positions of steps are indicated by arrows). From figure 3(a), we can notice that the first domain is formed at a field of 9 mT. The domain wall is pinned at the first junction until a reversal field of 16 mT is applied. The domain wall moves to the next junction only at a reversal field of 21 mT and so on. These results confirm our understanding

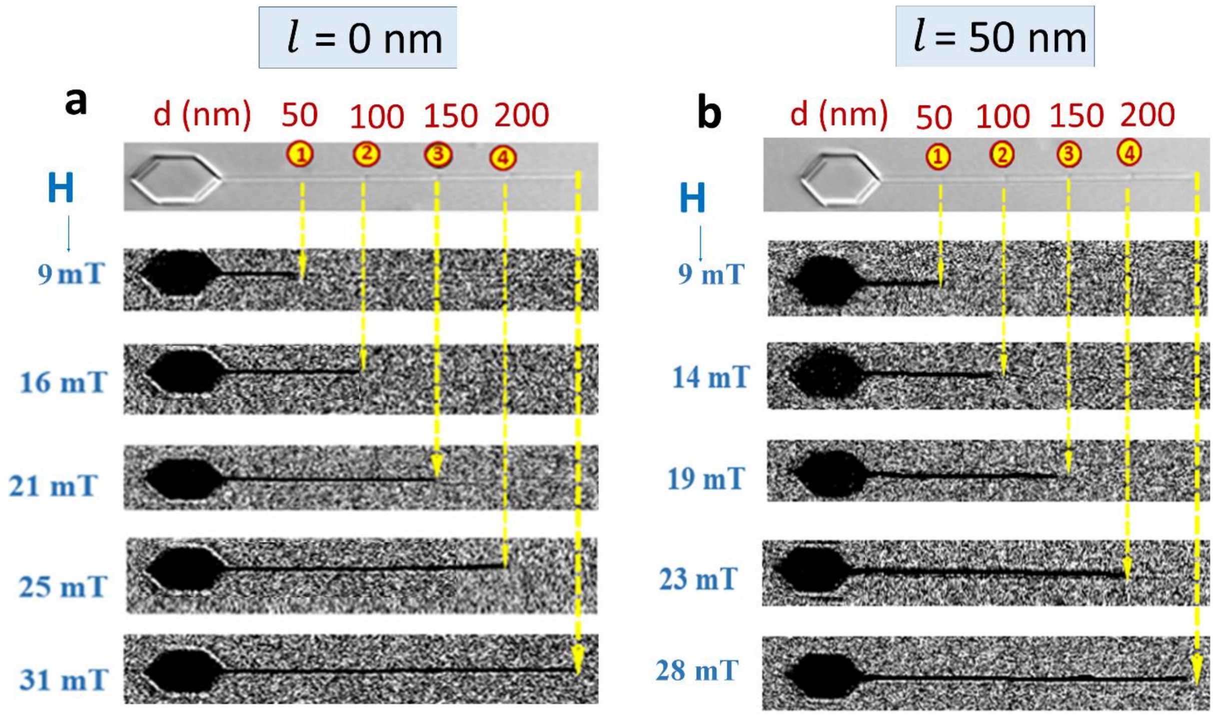

FIG. 3. The fabricated device with (a) l = 0 and (b) l = 50 nm. The values of d were varied from 50 to 200 nm with a step of 50 nm. The sample was first saturated at 30 mT in one direction then a reversed field was applied in the opposite direction. The depinning feld is indicated at the left side of each figure. The length and width of the nanowire are 75µm and 200 nm, respectively.

that the pinning strongly depends on l and d. The improved device design with increasing values of d helps to control the pinning at each junction precisely.

Figure 3(b) shows similar images for nanowires with step dimensions of l = 50 nm and various d values. We notice, in this case also, that the pinning strength and the depinning field depend on the junction as for the nanowire with l = 0 nm. However, the depinning field in this case is slightly smaller than what was observed with l = 0 nm. This can be understood based on the schematics shown in figure 1(g) and 1(h). For the case of l = 0 nm [Fig.1(g)], the width of the constriction region is w–d, where w is the width of the nanowire. However, for the case of l > 0 nm [Fig.1(h)], the width of the constriction is $\sqrt{(w-d)^2+l^2}$, which is larger than the case of l = 0 nm. As the effective constriction is narrower in the case of l = 0 nm, it provides the largest pinning field. We also carried out similar measurements for nanowires with a thicker NiFe layer (30 nm), to understand the effect of thickness. Figure 4 shows the domain observation trend for different values of the reversal magnetic field. We noticed that the depinning field is generally larger for thicker NiFe layers (about 30%).

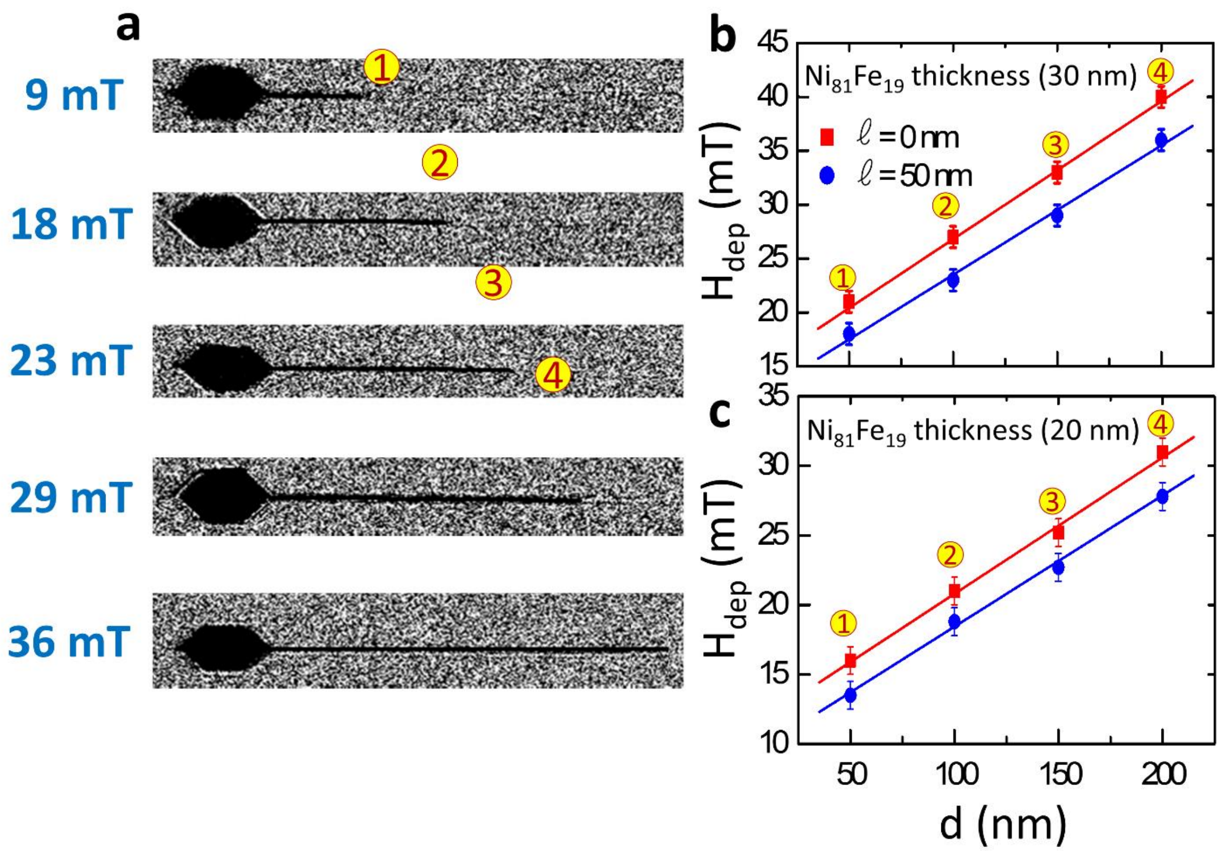

FIG. 4. (a) Magnetooptical images of domain wall motion for staggered NiFe (30 nm) with l = 0 and different values of d. The numbers indicate the position of staggered regions where domain wall was pinned precisely as the applied magnetic field is increased. The depinning field as a function of d for two different values of l for (b) the case of 30 nm thick NiFe and (c) for the case of 20 nm thick NiFe.

We show in figure 4b, the dependence of depinning field (H_{dep}) for various values of l and d. We can notice that the H_{dep} increases linearly with d. Similar result was observed for the case of 20 nm thick permalloy [Fig. 4(c)]. The trend is the same irrespective of the values of l. However, for a constant d, the depinning is the largest for l = 0 nm. These results are consistent with the schematic shown in figure 1(g-h).

After observing that the staggered nanowire is effective in pinning the domain walls, we proceeded to examine the stability of the domains formed at the junctions. For this purpose, we used MOKE set up observation in the presence of an in-plane magnetic field. Firstly, we saturated the sample at a magnetic field of 30 mT applied along one direction to saturate the magnetization in that direction. Then, we applied a reversal field and waited for a certain time τ, after which the domain moved. We saturated the sample again and increased the reversal field by 1 mT and observed the relaxation time for the domain wall to be displaced from the pinning site. We carried out this investigation of relaxation time (τ) versus the applied reversal magnetic field (H) for

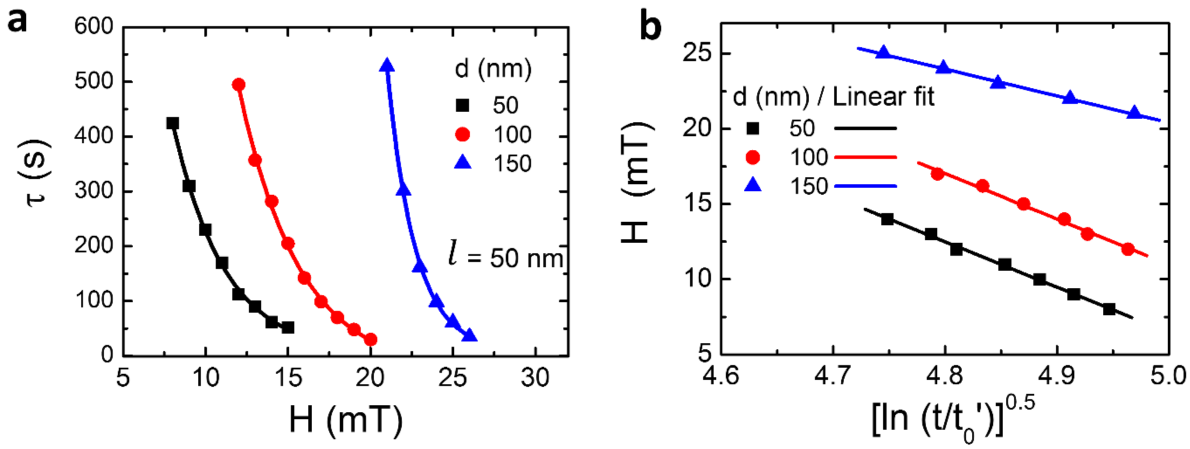

FIG. 5. (a) Relaxation time versus applied magnetic field for staggered nanowires with 30 nm-thick NiFe. For a given applied magnetic field, staggered nanowire with larger *d* are more stable. (b) The applied magnetic field as a function of relaxation time following Eq. (2) for α = 2.

values less than that of depinning field. Figure 5 (a) shows the relaxation time τ, for various values of *H*. We notice that the relaxation time is shorter for larger values of reversal field and that the values of τ and *H* follows the relation shown in Eq. (1) [46–48].

$$\tau = \tau'_0 \, exp\left[\frac{K_u V}{k_B T}\left(1 - \frac{H}{H_0}\right)^{\alpha}\right] \qquad (1)$$

$$H = H_0 - H_0\left(\frac{k_B T}{K_u V}\right)^{1/\alpha}\left[ln\left(\frac{\tau}{\tau'_0}\right)\right]^{1/\alpha} \qquad (2)$$

where $\tau_0{}'$ is the inverse of the attempt time with the value of 10^{-8} s, k_B is Boltzman constant and H_0 is the intrinsic depinning field. Equation (1) can be derived to yield equation (2). In order to estimate the stability of this device, we plotted *H* vs $(\ln(\frac{\tau)}{\tau_0'}))^{1/\alpha}$ which follows the linear relationship, shown in FIG. 5(b). Table 1 summarizes various properties obtained from the fitting. From the fitted data to equation 2, it was found that the domain stability for *d* =150 nm was about one and half years. For materials with higher anisotropy, the stability could be increased. It is also expected that the stability could be increased by reducing *l*.

To understand the types of domains formed in these nanowires, we also inspected the magnetic domain patterns of the samples using magnetic force microscope (MFM). In figures 6 (a & b), we show MFM images of two junctions. We can notice a bright spot at the centre of the junction in both the images, indicating the emergence of magnetic flux.

Table 1. Properties obtained from the fit of experimental data to equation 2, for α = 1.5. The values of the three fitting parameters do not differ much with α for *d*= 50 and 100 nm, except for *d*= 150 nm where an increase could be seen.

d (nm)	**50**	**100**	**150**
H_0 (T)	0.131	0.135	0.089
K_uV/k_BT	27	28.6	37.8
Stability	528 s	2220 s	300 days

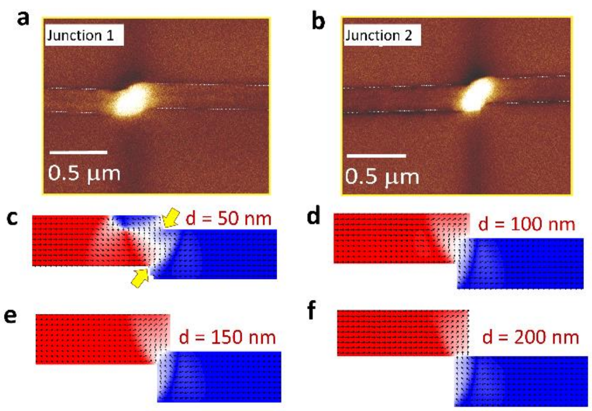

FIG. 6. (a and b) MFM images of stable domain wall at the first and second junction of staggered NiFe (20 nm). (c-f) Micromagnetic simulation images for devices with l = 50 and different d values. The two yellow arrows indicate the effective width of the junction as described in Fig. 1(h).

However, from the images it was not clear which type of domain is formed at these junctions. Therefore, we carried out micromagnetic simulations of the junctions for different values of *d*, using OOMMF [26]. Same material parameters and dimensions as in experiments were used in the simulation. Four junctions with l = 50 nm and d = 50, 100, 150 and 200 nm were simulated. The mesh size was fixed to 5 nm × 5 nm × 5 nm, sufficiently smaller than the exchange length of NiFe (~ 5.3 nm). DWs were created at the reservoir first, then depinned in to the nanowire to form domains as shown in Fig. 6 (c–f). We notice that the domain wall type and spin structure formed at the junction depends on the design parameters. For d = 50 nm, we observe a vortex DW (VDW). For larger values of d (100 nm and above), a transverse DW (TDW) was observed. The arrows in each graph indicate the magnetic moment directions for the left and right arms, respectively. Snapshot images of the stepped nanowire with different constriction sizes of l = 50 nm: (c) d =50 nm, (d) d =100 nm (e) d =150 nm and (f) d =200 nm shows DW is pinned at the stepped area. We also used micromagnetic simulations to estimate the domain wall velocity. Figure 7 shows magnetization component (m_x) along the wire direction as a function of time for devices with various values of *d*. The slope of this graph gives the rate of change of magnetization, or in other words, domain wall displacement as a function of time. It can be noticed that the slope is almost the same for all the devices. Considering that the length of a nanowire segment is 15 μm and that it takes about 70 ns for the domain wall to cross this distance, we determined the DW velocity to be about 200 m/s, which is in a reasonable range for

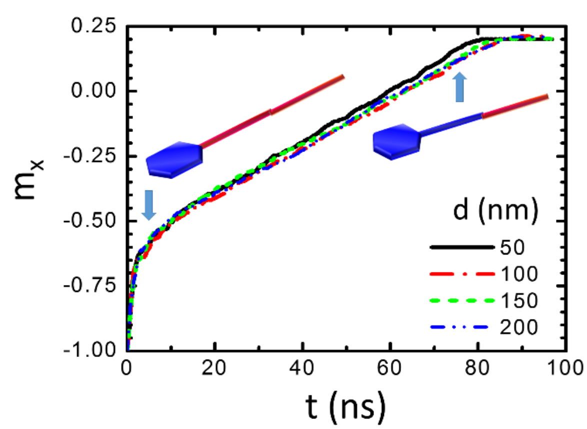

FIG. 7. Normalized x-component of NiFe (30nm) nanowire magnetization as a function of time for devices shown in Fig. 6(c-f). The left bold arrow indicate the position of domain wall at the right side of reservoir and the right bold arrow indicate the position of the domain wall at the junction region. Domain wall moves with a constant velocity of about 200 m/s.

applications in DW devices as previously shown experimentally [4]. These results also indicate that the DW velocity is independent of d or indirectly, the pinning strength.

IV. SUMMARY

We have proposed and demonstrated the use of staggered domain wall nanowires for effective tunable and controlled pinning of domain walls. We have observed the DW movement using MOKE for various applied field. We found that domain wall depinning field (H_{dp}) depends on the design parameters, l and d and the thickness of the NiFe layer investigated in this work. We also investigated the stability of DWs by relaxation time measurements and noticed an exponential dependence between DW relaxation time and the applied magnetic field that allows us to extract stabilities over years for the pinned domain walls. In addition, we have investigated the DW type by MFM and micromagnetic simulation, and found that the domain wall type depends on the geometry of the junction. Finally, domain wall velocities of 200 m/s can be expected for these devices showing that the combination of fast domain and controlled pinning can lead to good device performance.

[1] W. Wernsdorfer, B. Doudin, D. Mailly, K. Hasselbach, A. Benoit, J. Meier, J.-Ph. Ansermet, and B. Barbara, Nucleation of Magnetization Reversal in Individual Nanosized Nickel Wires, Phys. Rev. Lett. **77**, 1873 (1996).

[2] D. A. Allwood, G. Xiong, C. C. Faulkner, D. Atkinson, D. Petit, and R. P. Cowburn, Magnetic Domain-Wall Logic, Science **309**, 1688 (2005).

[3] M. P. Kostylev, A. A. Serga, T. Schneider, B. Leven, and B. Hillebrands, Spin-wave logical gates, Appl. Phys. Lett. **87,** 153501 (2005).

[4] M. Kläui, H. Ehrke, U. Rüdiger, T. Kasama and R. E. Dunin-Borkowski, D. Backes, L. J. Heyderman, C. A. F. Vaz and J. A. C. Bland, G. Faini and E. Cambril, and W. Wernsdorfer, Direct observation of domain-wall pinning at nanoscale constrictions, Appl. Phys. Lett. **87**, 102509 (2005).

[5] G. S. D. Beach, C. Nistor, C. Knutson, M. Tsoi, and J. L. Erskine, Dynamics of field-driven domain-wall propagation in ferromagnetic nanowires, Nature Mater. **4,** 741 (2005).

[6] M. Hayashi, L. Thomas, C. Rettner, R. Moriya, X. Jiang, and S. S. P. Parkin, Dependence of Current and Field Driven Depinning of Domain Walls on Their Structure and Chirality in Permalloy Nanowires, Phys. Rev. Lett. **97**, 207205 (2006).

[7] A. Khitun, D. E. Nikonov, M. Bao, K. Galatsis, and K. L. Wang, Feasibility study of logic circuits with a spin wave bus, Nanotechnology **18,** 465202 (2007).

[8] T. Schneider, A. A. Serga, B. Leven, and B. Hillebrands, Realization of spin-wave logic gates, Appl. Phys. Lett. **92,** 022505 (2008).

[9] S. S. P. Parkin, M. Hayashi, L. Thomas, Magnetic Domain-Wall Racetrack Memory, Science **320**, 190 (2008).

[10] L. O'Brien, D. E. Read, H. T. Zeng, E. R. Lewis, D. Petit, and R. P. Cowburn, Bidirectional magnetic nanowire shift register, Appl. Phys. Lett. **95**, 232502 (2009).

[11] M. Diegel, S. Glathe, R. Mattheis, M. Scherzinder, and E. Halder, A New Four Bit Magnetic Domain Wall Based Multiturn Counter, IEEE Trans. Magn. **45**, 3792 (2009).

[12] T. H. E. Lahtinen, K. J. A. Franke, and S. van Dijken, Electric-field control of magnetic domain wall motion and local magnetization reversal, Sci. Rep. **2**, 258 (2012).

[13] H. Tanigawa, T. Suzuki, S. Fukami, K. Suemitsu, N. Ohshima, and E. Kariyada, Thickness dependence of current-induced domain wall motion in a Co/Ni multi-layer with out-of-plane anisotropy, Appl. Phys. Lett. **102**, 152410 (2013).

[14] A. Fernandez-Pacheco, L. Serrano-Ramón, J. M. Michalik, M. R. Ibarra, J. M. De Teresa, L. O'Brien, D. Petit, J. Lee, and R. P. Cowburn, Three dimensional magnetic nanowires grown by focused electron-beam induced deposition, Sci. Rep. **3**, 1492 (2013).

[15] R. Sbiaa, and S. N. Piramanayagam, Multi-level domain wall memory in constricted magnetic nanowires, Appl. Phys. A **114**, 1347 (2014).

[16] B. Van de Wiele, L. Laurson, K. J. A. Franke, and S. van Dijken, Electric field driven magnetic domain wall motion in ferromagnetic-ferroelectric heterostructures, Appl. Phys. Lett. **104**, 012401 (2014).

[17] J.-S. Kim, M.-A. Mawass, A. Bisig, B. Krüger, R. M. Reeve, T. Schulz, F. Büttner, J. Yoon, C.-Y. You, M. Weigand, H. Stoll, G. Schütz, H. J. M. Swagten, B. Koopmans, S. Eisebitt, and M. Kläui, Synchronous precessional motion of multiple domain walls in a ferromagnetic nanowire by perpendicular field pulses, Nat. Commun. **5**, 3429 (2014).

[18] M. Al Bahri, and R. Sbiaa, Geometrically pinned magnetic domain wall for multi-bit per cell storage memory, Sci. Rep. **6**, 28590 (2016).

[19] A. Bisig, L. Heyne, O. Boulle, and M. Kläui,.Tunable steady-state domain wall oscillator with perpendicular magnetic anisotropy, Appl. Phys. Lett. **95,** 162504 (2009).

[20] G. Gubbiotti, S. Tacchi, G. Carlotti, N. Singh, S. Goolaup and A. O. Adeyeye, and M. Kostylev, Collective spin modes in monodimensional magnonic crystals consisting of dipolarly coupled nanowires, Appl. Phys. Lett. **90,** 092503 (2007).

[21] A. V. Chumak, A. A. Serga, B. Hillebrands, and M. P. Kostylev, Scattering of backward spin waves in a one-dimensional magnonic crystal, Appl. Phys. Lett. **93,** 022508 (2008).

[22] S.-K. Kim, K.-S. Lee, and D. –S. Han, A gigahertz-range spin-wave filter composed of width-modulated nanostrip magnonic-crystal waveguides, Appl. Phys. Lett. **95,** 082507 (2009).

[23] R. Sbiaa, and R. Chantrell, Domain wall oscillations induced by spin torque in magnetic nanowires, J. Appl. Phys. **117**, 053907 (2015).

[24] B. Van de Wiele, S. J. Hämäläinen, P. Baláẑ, F. Montoncello, and S. van Dijken, Tunable short-wavelength spin wave excitation from pinned magnetic domain walls, Sci. Rep. **6**, 21330 (2016).

[25] R. Sbiaa, M. Al Bahri, and S.N. Piramanayagam, Domain wall oscillation in magnetic nanowire with a geometrically confined region, J. Magn. Magn. Mat. **456**, 324 (2018).

[26] K.-S. Lee, and S.-K. Kim, Conceptual design of spin wave logic gates based on a Mach–Zehnder-type spin wave interferometer for universal logic functions, J. Appl. Phys. **104,** 053909 (2008).

[27] M. Jamali, J. H. Kwon, S. -M. Seo, K. -J. Lee, and H. Yang, Spin wave nonreciprocity for logic device applications, Sci. Rep. **3,** 3160 (2013).

[28] B. Borie, A. Kehlberger, J. Wahrhusen, H. Grimm, and M. Kläui, Geometrical Dependence of Domain-Wall Propagation and Nucleation Fields in Magnetic-Domain-Wall Sensors, Phys. Rev. Applied **8**, 024017 (2017).

[29] M. Okuda, Y. Miyamoto, E. Miyashita, N. Saito, N. Hayashi, and S. J. Nakagawa, Detection of current-driven magnetic domains in [Co/Pd] nanowire by tunneling magnetoresistive sensor, J. Appl. Phys. **117**, 17D516 (2015).

[30] O. Boulle, G. Malinowski, and M. Kläui, Current-induced domain wall motion in nanoscale ferromagnetic elements, Mater. Sci. Eng. R72, 159 (2011).

[31] L. K. Bogart, D. Atkinson, K. O'Shea, D. McGrouther, and S. Mc Vitie, Dependence of domain wall pinning potential landscapes on domain wall chirality and pinning site geometry in planar nanowires, Phys. Rev **B79**, 054414 (2009).

[32] K. Xu, D. K. Schreiber, Y. L. Li, B. R. Johnson, and J. McCloy, Effect of defects, magnetocrystalline anisotropy, and shape anisotropy on magnetic structure of iron thin films by magnetic force microscopy, AIP Adv. **7**, 056806 (2017).

[33] D. Castilla, M. Maicas, J. L. Prieto, and M. P. J. Proenca, Depinning process of magnetic domain walls in cylindrical nanowires with a chemical constraint, J. Phys. D-Appl. Phys. **50**,105001 (2017).

[34] M. Hayashi, L. Thomas, C. Rettner, R. Moriya, X. Jiang, and S. S. P. Parkin, Dependence of Current and Field Driven Depinning of Domain Walls on Their Structure and Chirality in Permalloy Nanowires, Phys. Rev. Let .**97**, 207205 (2006).

[35] D. Petit, A. -V Jausovec, D. Read, and R. P. J. Cowburn, Domain wall pinning and potential landscapes created by constrictions and protrusions in ferromagnetic nanowires, J. Appl. Phys. **103,** 114307 (2008).

[36] S.-H. Huang, and C. -H. Lai, Domain-wall depinning by controlling its configuration at notch, Appl. Phys. Lett. **95**, 032505 (2009).

[37] L. K. Bogart, D. Atkinson, K. O'Shea, D. McGrouther, and S. McVitie, Dependence of domain wall pinning potential landscapes on domain wall chirality and pinning site geometry in planar nanowires, Phys. Rev. **B79**, 054414 (2009).

[38] E. Berganza, C. Bran, M. Jaafar, M. Vázquez, and A. Asenjo, Domain wall pinning in FeCoCu bamboo-like nanowires, Sci. Rep. **6**, 29702 (2016).

[39] A. Ding, I. Will, C. Lu, and Y. B. Xu, Vortex Domain Wall Formation in Nanowires With Twin Pinning Sites, IEEE Trans. Magn. **48,** 2304 (2012).

[40] U. Bauer, S. Emori, and G. S. D. Beach, Voltage-controlled domain wall traps in ferromagnetic nanowires, Nature Nanotech. **8**, 411 (2013).

[41] Y. Gao, B. You, X. Z. Ruan, M. Y. Liu, H. L. Yang, Q. F. Zhan, Z. Li, N. Lei, W. S. Zhao, D. F. Pan, J. G. Wan, J. Wu, H. Q. Tu, J. Wang, W. Zhang, Y. B. Xu, and J. Du, Depinning of domain walls in permalloy nanowires with asymmetric notches, Sci. Rep. **6**, 32617 (2016).

[42] D. Backes, C. Schieback, M. Kläui, F. Junginger, H. Ehrke, P. Nielaba, U. Rüdiger, L. J. Heyderman, C. S. Chen, T. Kasama, R. E. Dunin-Borkowski, C. A. F. Vaz, and J. A. C. Bland, Transverse domain walls in nanoconstrictions, Appl. Phys. Lett. **95**, 112502 (2007).

[43] S. Bhatti, R. Sbiaa, A. Hirohata, H. Ohno, S. Fukami, and S.N.Piramanayagam, 5. Spintronics based Random Access Memory: A Review, Mat. Today **20**, 530 (2017).

[44] T. L. Jin, M. Ranjbar, S. K. He, W. C. Law , T. J. Zhou, W. S. Lew, X. X. Liu, and S. N. Piramanayagam, Tuning magnetic properties for domain wall pinning via localized metal diffusion, Sci. Rep. **7** 16208 (2017).

[45] I. Polenciuc, A. J. Vick, D. A. Allwood, T. J. Hayward, G. Vallejo-Fernandez, K. O'Grady, and A. Hirohata, Domain wall pinning for racetrack memory using exchange bias, Appl. Phys. Let. **105**, 162406 (2014).

[46] M. P. Sharrock, Time dependence of switching fields in magnetic recording media, J. Appl. Phys.**76**, 6413 (1994).

[47] H. J. Richter, S. Z. Wu, and R. Malmhall, IEEE Trans. Magn. **34**, 1540 (1998).

[48] S. N. Piramanayagam, Perpendicular recording media for hard disk drives, J. Appl. Phys. **102**, 011301 (2007).